



**University of  
Zurich**<sup>UZH</sup>

**Zurich Open Repository and  
Archive**

University of Zurich  
University Library  
Strickhofstrasse 39  
CH-8057 Zurich  
[www.zora.uzh.ch](http://www.zora.uzh.ch)

---

Year: 2004

---

## **Long-term MERIS land product accuracy assessment based on vicarious calibration and regional validation**

Zurita-Milla, Raúl ; Schaepman, Michael E ; Clevers, Jan G P W ; Kneubühler, Mathias ; Delwart, Steven

**Abstract:** Since the launch of MERIS on board of ENVISAT long term activities using vicarious calibration approaches have been set in place to monitor potential drifts in the calibration of the radiance products of MERIS. In this paper, a stable and well monitored reference calibration site named Railroad Valley Playa (Nevada, USA) is used to derive the calibration uncertainties of the MERIS FR TOA radiance over time. Subsequently, a linear interpolation of these uncertainties is performed for a set of images covering the whole of the Netherlands (which is used as a validation site). After this, the images over the Netherlands were corrected on the basis of the previously interpolated uncertainties and classified in 9 land use classes using linear spectral unmixing and matched filtering techniques. The classification endmembers were derived from an image-based land use map of the Netherlands (LGN4) after determining the most homogeneous areas for each land use type by means of a standard purity index and a moving window filter to minimize possible adjacency effects. Finally, the impact of the calibration accuracy over the land use classification is assessed by comparing classification results both for corrected and uncorrected images. We conclude that the classification performance may significantly be increased, when taking into account long-term vicarious calibration results.

Posted at the Zurich Open Repository and Archive, University of Zurich

ZORA URL: <https://doi.org/10.5167/uzh-98424>

Conference or Workshop Item

Published Version

Originally published at:

Zurita-Milla, Raúl; Schaepman, Michael E; Clevers, Jan G P W; Kneubühler, Mathias; Delwart, Steven (2004). Long-term MERIS land product accuracy assessment based on vicarious calibration and regional validation. In: ENVISAT ERS Symposium, Salzburg, Austria, 6 September 2004 - 10 September 2004. European Space Agency \* Communication Production Office, 63-71.

# LONG-TERM MERIS LAND PRODUCT ACCURACY ASSESSMENT BASED ON VICARIOUS CALIBRATION AND REGIONAL VALIDATION

R. Zurita Milla<sup>(1)</sup>, M.E. Schaepman<sup>(1)</sup>, J.G.P.W. Clevers<sup>(1)</sup>, M. Kneubuehler<sup>(2)</sup> and S. Delwart<sup>(3)</sup>

(1) Centre for Geo-Information (CGI), Wageningen University. P.O.Box 47. 6700AA Wageningen (The Netherlands). Email: Raul.Zurita@wur.nl

(2) Remote Sensing Laboratories (RSL), University of Zurich. Winterthurerstr. 190. 8057 Zurich (Switzerland). Email: kneub@geo.unizh.ch

(3) ESA/ESTEC. Keplerlaan 1. P.O.Box 299. 2200AG Noordwijk (The Netherlands). Email: steven.delwart@esa.int

## ABSTRACT

Since the launch of MERIS on board of ENVISAT long term activities using vicarious calibration approaches have been set in place to monitor potential drifts in the calibration of the radiance products of MERIS. In this paper, a stable and well monitored reference calibration site named Railroad Valley Playa (Nevada, USA) is used to derive the calibration uncertainties of the MERIS FR TOA radiance over time. Subsequently, a linear interpolation of these uncertainties is performed for a set of images covering the whole of the Netherlands (which is used as a validation site). After this, the images over the Netherlands were corrected on the basis of the previously interpolated uncertainties and classified in 9 land use classes using linear spectral unmixing and matched filtering techniques.

The classification endmembers were derived from an image-based land use map of the Netherlands (LGN4) after determining the most homogeneous areas for each land use type by means of a standard purity index and a moving window filter to minimize possible adjacency effects.

Finally, the impact of the calibration accuracy over the land use classification is assessed by comparing classification results both for corrected and uncorrected images. We conclude that the classification performance may significantly be increased, when taking into account long-term vicarious calibration results.

## 1. INTRODUCTION

The Medium Resolution Imaging Spectrometer (MERIS) [1] is one of totally ten instruments on board ESA's ENVISAT platform [2, 3]. MERIS is a 68.5° field-of-view pushbroom imaging spectrometer that measures the solar radiation reflected by the Earth, at a ground spatial resolution of 300 m in full resolution (FR) and 1200 m at reduced resolution (RR). MERIS

has 15 spectral bands covering the visible and near infra-red region of the electromagnetic spectrum and it allows global coverage of the Earth in 3 days. MERIS data products provided by ESA include georeferenced TOA radiance data (Level 1b) as well as various water [4], land [5, 6] and atmospheric products [7, 8] (Level 2), as well analytical tools for end users to access the data [9, 10]. The radiometric data quality of MERIS [11] is based on several calibration efforts, including on-board diffuser calibration [12, 13] and vicarious calibration [14, 15, 16], amongst others. The latest calibration results that include the treatment of all the above efforts are used in this paper to demonstrate the impact of the calibration accuracy of the MERIS Level 1b TOA radiance on the classification accuracy of a large area: The Netherlands.

## 2. METHODS AND DATA CALIBRATION

### 2.1 Vicarious calibration

Vicarious calibration is an independent method for monitoring instrument radiometric performance, including error assessment with reflectance standards, field instruments and atmospheric radiation measurements simultaneous to the satellite overpass [17]. In other words, vicarious calibration includes all the relevant steps required to convert raw sensor data into accurate and useful radiometric quantities without making use of the satellite on-board calibration sources.

This particular experiment follows a so called reflectance-based approach with ground measurements of the atmospheric optical depth and surface reflectance over a bright natural target. In this way, the calibration uncertainties at the top of atmosphere level (TOA) can be computed and, subsequently, extrapolated to acquisition orbits located in-between of two given vicarious calibration attempts by assuming that the

radiometric uncertainty remains stable (e.g., linearly interpolable) between these acquisitions. This approach follows in certain ways the so called QUASAR [18, 19] approach, but does not support simultaneous airborne instrument acquisitions.

### 2.1.1 Railroad Valley Playa Test Site

The dry lakebed of Railroad Valley Playa (RRVP), Nevada, USA is located at 1.35 km above sea level (38.504° N latitude, 115.692° W longitude). It is a desert site with no vegetation. Temporal records for this site show reflectance variations as a function of time of year, with lowest reflectance in the winter months due to a rising water table. The accuracy of vicarious calibration experiments over land is highly dependent on the choice of an appropriate calibration target. Ideally, such a calibration site should be flat, bright, spatially uniform, and spectrally stable over time, near Lambertian for small angles off nadir, and of sufficiently large spatial extent. Desert playas are preferred for vicarious calibration of moderate spatial resolution sensors due to their optical properties, predictably sunny conditions and low atmospheric aerosol loading. In this experiment, in-situ sun photometer data from all dates of MERIS acquisitions were available. MODTRAN-4 [20, 21], a radiative

transfer code (RTC) is used, constrained by field data, to calculate the top-of-atmosphere radiance present at the sensor. Input parameters include ground measurements of the surface reflectance, sun-target-sensor geometries and atmospheric properties (aerosol model, horizontal visibility). The method is described in detail in [14].

Using the data collected at RRVP, the relative mean error (RME) for each spectral band of MERIS was calculated in the following way:

$$RME^i (\%) = 100 \cdot \left( \frac{L_{MERIS\_TOA}^i - L_{VC\_TOA}^i}{L_{MERIS\_TOA}^i} \right) \quad (1)$$

Where:  $L_{MERIS\_TOA}^i$  is the MERIS FR level 1b TOA radiance for band  $i$  and  $L_{VC\_TOA}^i$  is the simulated TOA radiance for the same band based on the ground measurements

Fig. 1 illustrates in detail the achieved vicarious calibration uncertainty for each spectral band of MERIS. The bands affected most by the atmosphere (e.g., 11 and 15) have been rescaled due to the larger uncertainties present in these graphs.

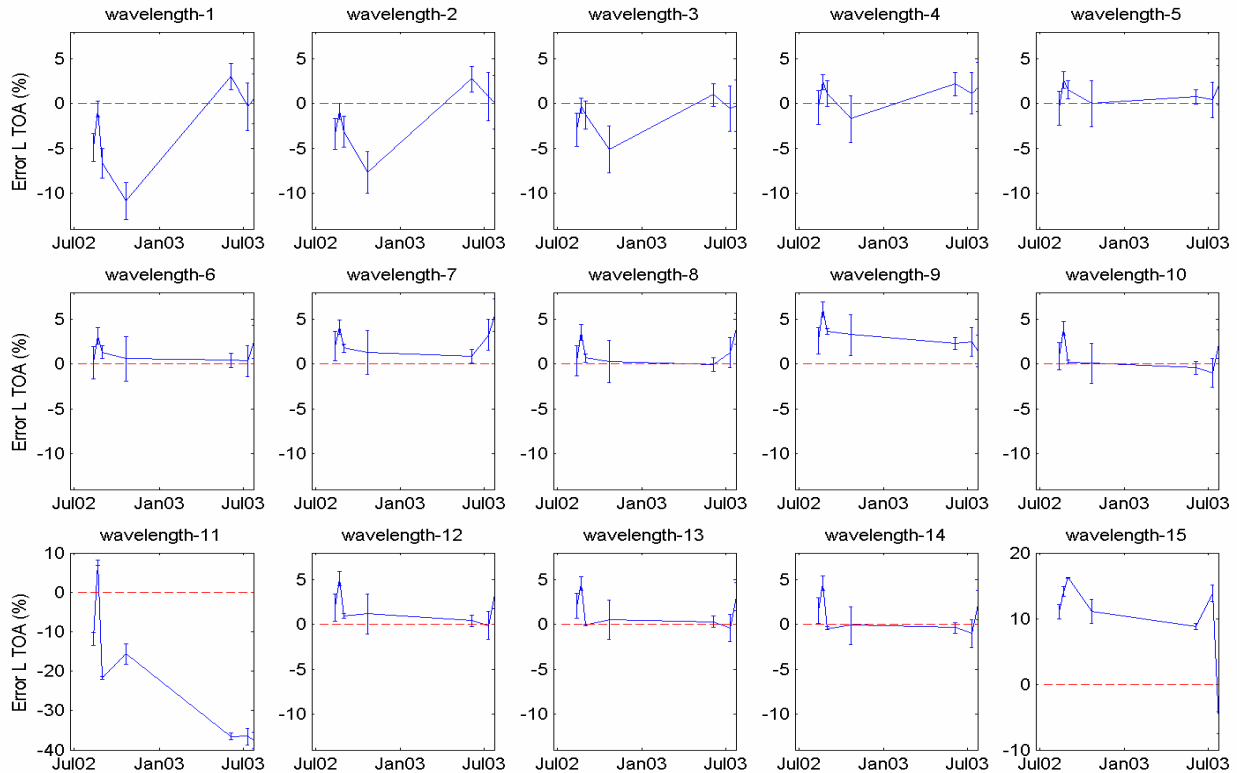


Fig. 1: Temporal evolution of calibration uncertainty for vicarious calibration in all 15 MERIS spectral bands between July 2002 and July 2003. RME errors are plotted on the y-axis, and band 11 and 15 have different y-axis scaling than the other bands.

## 2.2 MERIS data availability and processing

For this particular experiment, programming requests were scheduled to acquire MERIS FR (Full Resolution) 1b data over RRVP and the Netherlands. Fig. 2 lists all the MERIS acquisitions that have been made. Out of 32 full coverage's of the Netherlands between July 2002 and April 2004 (top line), 11 were considered to be cloud free (second line from top, less than 1/8 cloud cover) and three scenes have finally been selected as reference (bottom line). The further reduction by 8 scenes is a result of partial cloud cover or the fact that the images were not covering the whole of the Netherlands. In the same period 7 acquisitions in RRVP have been taken place (second line from bottom), such that sufficient scenes were available to propagate uncertainties in a linear way.

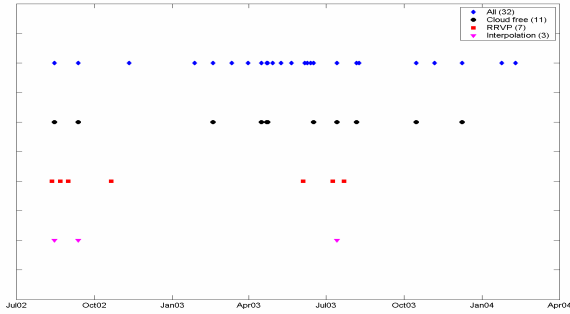


Fig. 2: MERIS FR Level 1b acquisitions over the Netherlands (top two and bottom line), as well as Railroad Valley Playa (second line from bottom). 7 RRVP and 3 Netherlands scenes were finally selected for further processing.

Table 1 summarizes the dates for the three images of the Netherlands used in this study and the six RRVP calibration dates employed to do the linear interpolation of the vicariously derived calibration uncertainties.

Table 1: Dates used for the uncertainty analysis

Date	The Netherlands	RRVP
12/08/2002		X
15/08/2002	X	
22/08/2002		X
31/08/2002		X
12/09/2002	X	
21/10/2001		X
09/07/2003		X
14/07/2003	X	
22/07/2003		X

After interpolating the mean radiometric uncertainties (mean RMSE) for each band of the three images of the Netherlands, a vicarious correction factor could be computed and applied to generate vicariously corrected images from the original images. Following eq. 1 the correction factor depicted in Table 2 was calculated as follow:

$$L_{MERIS\_VC}^i = L_{VC\_TOA}^i = L_{MERIS\_TOA}^i \cdot \left(1 - \frac{RME^i}{100}\right) \quad (2)$$

Where:  $L_{MERIS\_VC}^i$  is the corrected ('true') value for the MERIS TOA radiance for the band  $i$ , which is assumed to be equal to the  $L_{VC\_TOA}^i$  value.

Table 2: MERIS FR Level 1b correction factors interpolated from RRVP vicarious calibration experiments to acquisitions in the Netherlands.

Band	15/08/2002	12/09/2002	14/07/2003
1	1.0360	1.0762	0.9999
2	1.0260	1.0420	0.9947
3	1.0208	1.0216	1.0042
4	0.9954	0.9951	0.9858
5	0.9953	0.9882	0.9892
6	0.9891	0.9884	0.9882
7	0.9736	0.9831	0.9591
8	0.9869	0.9942	0.9765
9	0.9631	0.9643	0.9791
10	0.9822	0.9981	0.9973
11	1.0597	1.2024	1.3689
12	0.9710	0.9900	0.9876
13	0.9715	0.9989	0.9903
14	0.9753	1.0035	0.9972
15	0.8800	0.8499	0.9376

In addition to the radiometric correction, the images were reprojected into the Dutch National reference coordinate system (RD) and overlaid with a vector map of coast boundaries to assess the co-registration accuracy of the three acquisition dates. Visual interpretation of the images indicated that the number of ground control points provided with the images were sufficient to perform a good image registration.

### 2.3 Land use database

For the Netherlands, the Dutch land use database (LGN) is used as reference. The database uses a grid structure with a cell size of 25 meters; the scale is about 1:50.000. The nomenclature of the LGN4 database contains 39 classes covering urban areas, water, forest, various agricultural crops and ecological classes. LGN is created for an important part on the base of satellite imagery, but also other data sources are integrated into the database. Currently four versions exist ranging from LGN1 to LGN4, spanning a time period between 1986 and 2000. In this study we are using exclusively LGN4, which is based on satellite data of 1999 and 2000. The overall classification accuracy is (depending on class type) between 85-90 % [22].

The initial LGN4 is based on 39 land use classes, which were for MERIS aggregated into 9 main land cover classes. These classes are: grassland, arable land, greenhouses, deciduous forest, coniferous forest, water, built-up areas, bare soil (incl. sand dunes), and natural vegetation (c.f., Fig. 3, left).

In order to support the selection of pure endmembers, while using LGN4 as a reference, the database was resampled from 25 to 300 m to match the MERIS FR pixel size. The aggregation method is based on using a majority filter with a kernel size of 12 pixels (25 m \* 12 = 300m). The land use with the highest abundance in the 12 by 12 kernel was used to label the new land use type. Due to the very heterogeneous land use in the Netherlands, the proportion of every class within the kernel was also recorded during the aggregation process, such that a so called standard purity index (SPI) could be calculated from each window, as noted in eq. 3:

$$SPI = \sqrt{\frac{\sum_{i=1}^{i=n} (f_i - f_{\max class})^2}{n-1}} \quad (3)$$

Where:  $f$  represents the fraction of each land use in the kernel,  $f_{\max class}$  is the maximum fraction (the class driving the labeling process), and  $n$  is the number of classes. Consequently  $SPI = 1$ , when only one class is present in the kernel window.

A threshold of  $SPI = 0.9$  was defined as minimum criteria for all the classes except for the class greenhouses where SPI was fixed to 0.6 in order to get some pixels of this sparse land use type. After masking

out the most homogeneous pixels present in the LGN, a moving window filter of 3 by 3 pixels was applied in order to minimize possible adjacency effects. Thus, only ‘pure’ pixels surrounded by the same land use class were finally selected. Fig. 3 (bottom) displays all the pixels that are meeting the homogeneity criteria as developed above.

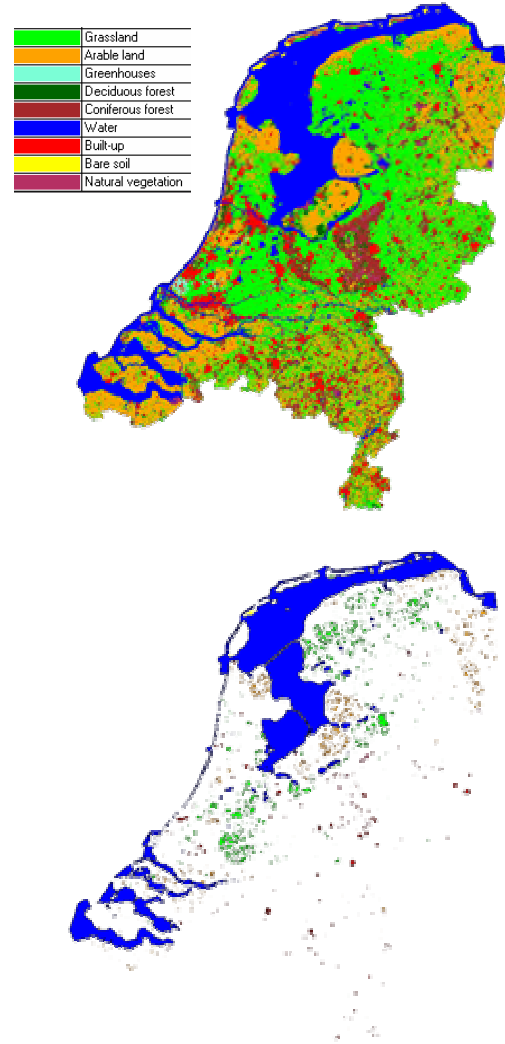


Fig. 3: Up: The Dutch land use database LGN4 aggregated into 9 land use classes and resampled to 300 m pixel size. Down: ‘Pure’ pixel selection in the Netherlands using the Standard Purity Index (SPI) and the moving window filter

### 2.4 Spectral unmixing

After having identified the proper location of homogenous areas in the Netherlands, for each one of

the nine classes the spectral signatures of the pure land use types, or endmembers, were derived. Fig. 4 plots as an example the spectral signatures derived from the image of 14<sup>th</sup> of July when using the locations identified over the LGN4. The corresponding numbers of 300 x 300 m pixels used to derive these endmembers are listed in Table 3.

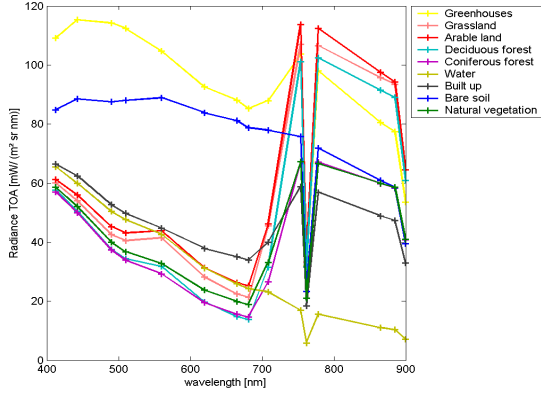


Fig. 4: Mean MERIS TOA spectral signatures of nine land use classes as defined in the LGN4 database.

Two unmixing methods were applied to assess the classification accuracy: unconstrained linear spectral unmixing [23, 24] and matched filtering [25]. The latter approach turned out to be very useful, since it maximizes the response of a known endmember and suppresses the response of the composite unknown background, thus matching the known signature. It also provides a rapid method of detecting specific classes based on matches to specific library or image endmember spectra. On the other hand, the linear spectral unmixing method offers the possibility of getting the root mean square error (RMSE) per pixel; error that can be seen as an index to quantify how well the endmembers are fitting the data

Table 3: Number of identified homogenous pixels per aggregated land use class in LGN4.

Land use	# pixels
Greenhouses	25
Grassland	4927
Arable land	2629
Deciduous forest	33
Coniferous forest	201
Water	58285
Built up areas	390
Bare soil	132
Natural vegetation	169

### 3. RESULTS

The three available MERIS images, both in their original form (N) and fully calibrated (VC), were classified using the linear spectral unmixing and the matched filtering methods. This choice, resulted in four possible combinations per classification method since the endmembers could be selected either from the same image (resulting in the cases N\_N or VC\_VC) or from the corrected image and applied to the uncorrected image and vice versa (i.e. the cross cases VC\_N and N\_VC).

Furthermore, due to increased atmospheric attenuation and large uncertainties, MERIS bands 1, 2, 11 and 15 were excluded from the analysis in a second classification, which was named after the number of bands finally used. The degrees of freedom and the dimensionality analysis nevertheless required do not allow choosing any number below 11 bands.

Tables 3 and 4 show the overall classification accuracy for the different combinations described above and for the two selected classification methods: the linear spectral unmixing and the match filtering.

Table 3: MERIS TOA classification accuracy performed for 9 land use classes based on the linear spectral unmixing approach.

Date	Image	Endmember	15 bands	11 bands
15_aug	N	N	23.36%	18.73%
15_aug	N	VC	11.20%	1.68%
15_aug	VC	N	15.77%	10.21%
15_aug	VC	VC	22.46%	18.72%
12_sep	N	N	25.12%	29.80%
12_sep	N	VC	16.94%	8.96%
12_sep	VC	N	28.81%	12.47%
12_sep	VC	VC	24.75%	29.83%
14_jul	N	N	25.98%	28.36%
14_jul	N	VC	1.67%	4.79%
14_jul	VC	N	9.35%	11.12%
14_jul	VC	VC	24.99%	35.37%

Table 4: MERIS TOA classification accuracy performed for 9 land use classes based on the matched filtering approach.

Date	Image	Endmember	15bands	11bands
15_aug	N	N	53.40%	52.90%
15_aug	N	VC	28.90%	32.41%
15_aug	VC	N	25.69%	36.22%
15_aug	VC	VC	53.40%	52.90%
12_sep	N	N	51.65%	50.91%
12_sep	N	VC	28.60%	38.04%
12_sep	VC	N	25.66%	38.15%
12_sep	VC	VC	51.65%	50.91%
14_jul	N	N	57.24%	57.27%
14_jul	N	VC	24.36%	40.86%
14_jul	VC	N	23.97%	44.14%
14_jul	VC	VC	57.24%	57.27%

Tables 5 and 6 indicate the mean and the standard deviation (SD) values for the RMSE of the unconstrained linear spectral unmixing approach for 15 and 11 spectral bands respectively. The standard deviation comes from the spatial distribution of this variable over the whole of the Netherlands (Fig. 5).

Table 5: Final RMSE values (mean plus standard deviation) for MERIS land use classification using 15 bands.

Date	Image	Endmember	RMSE	
			MEAN 15	SD 15
15_aug	N	N	0.227	0.353
15_aug	N	VC	1.344	0.701
15_aug	VC	N	1.336	0.651
15_aug	VC	VC	0.215	0.345
12_sep	N	N	0.227	0.353
12_sep	N	VC	1.344	0.701
12_sep	VC	N	1.336	0.651
12_sep	VC	VC	0.215	0.345
14_jul	N	N	0.192	0.182
14_jul	N	VC	1.582	0.626
14_jul	VC	N	1.833	0.729
14_jul	VC	VC	0.195	0.191

Table 6: Final RMSE values (mean plus standard deviation) for MERIS land use classification using 11 bands.

Date	Image	Endmember	RMSE	
			MEAN 11	SD 11
15_aug	N	N	0.086	0.326
15_aug	N	VC	0.163	0.328
15_aug	VC	N	0.135	0.327
15_aug	VC	VC	0.086	0.324
12_sep	N	N	0.086	0.326
12_sep	N	VC	0.163	0.328
12_sep	VC	N	0.135	0.327
12_sep	VC	VC	0.086	0.324
14_jul	N	N	0.088	0.106
14_jul	N	VC	0.205	0.114
14_jul	VC	N	0.179	0.104
14_jul	VC	VC	0.086	0.104

Finally, a potential processing artifact was found when examining the spatial distribution of the RMSE from the unconstrained linear spectral unmixing (Fig. 5). Such an artifact consists on a discrete line crossing The Netherlands from the North-East to the South-West and it could be due to discontinuities in the MERIS cameras calibration parameters or because the images used for this calibration experiment were not corrected for the so-called “smile effect”.

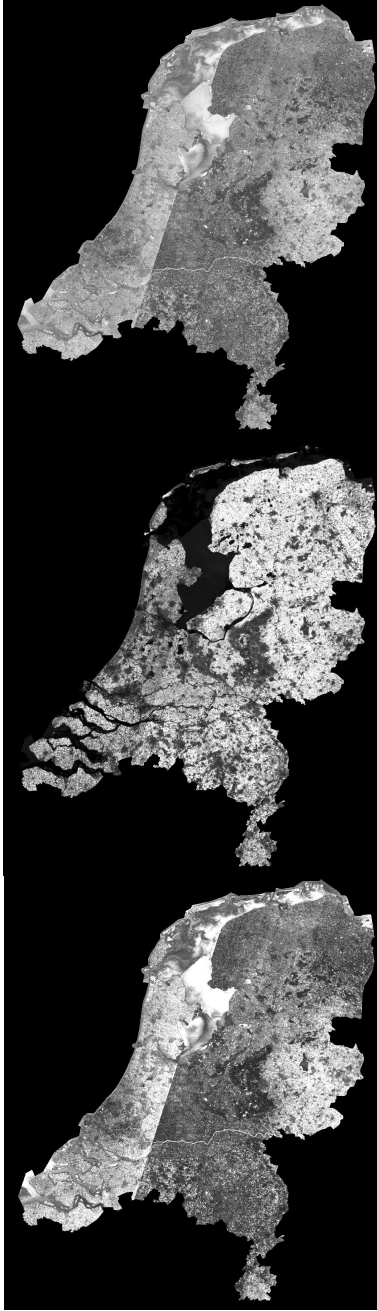


Fig. 5: Spatially distributed RMSE from unconstrained spectral unmixing for three endmember combinations (July 14). Up: Image based, uncalibrated (N\_N) endmembers; Middle: Calibrated endmembers applied on uncalibrated image (N\_VC), and Down: Image based calibrated (VC\_VC) endmember selection.

#### 4. CONCLUSIONS AND OUTLOOK

We have demonstrated a calibration approach based on MERIS data that can increase the classification accuracy of land use classes significantly. By assuming that non-vicariouly calibrated data are being used with well calibrated endmembers in comparison with well calibrated images and endmembers, the classification accuracy could be increased from 23.9% to 57.2% on July 14. Apparently this acquisition date has the best discrimination potential based on the spectral signatures of the 9 land use classes used. Nevertheless also for the other dates, the increase in classification accuracy can be considered as significant, though throughout with lower values.

The overall accuracy of 57% seems to be low in comparison to the achievement of LGN4 (90%), but it must be stated that neither a priori knowledge has been used for this approach, nor ancillary information.

By more closely examining the RMSE images a potential processing artifact is clearly visible in the form of a discrete line crossing The Netherlands. A discontinuity in the MERIS cameras calibration parameters or the “smile effect” could be the cause of this line. The MERIS data used for this calibration effort are currently being reprocessed using the latest version of the MERIS processor, which tentatively will remove the artifact.

The proposed method has been proven to be applicable to discrete land use classification data. Nevertheless, we plan to apply this method by using advanced error propagation methods to estimate the uncertainty of continuous data (eg such as the MERIS Terrestrial Chlorophyll Index (MTCI)), rather than on discrete land use/land cover data.

#### ACKNOWLEDGEMENTS

We would like to thank Carsten Brockmann from Brockmann Consult for timely MERIS data processing and delivery. Kurt Thome from the University of Arizona is thanked for providing ground data of the RRVP. The contribution of R. Zurita Milla is granted through the Dutch SRON GO programme (EO-061).



## REFERENCES

1. J.-L. Bézy, S. Delwart and M. Rast, *The esa medium resolution imaging spectrometer meris*, Proceedings of SPIE - The International Society for Optical Engineering **3439** (1998), 594-604.
2. H. Laur, G. Kohlhammer, Y. L. Desnos and S. Coulson, *The envisat mission: Access to the data*, International Geoscience and Remote Sensing Symposium (IGARSS) **1** (2002), 617-619.
3. J. Louet, *The envisat mission and system*, European Space Agency Bulletin (2001), no. 106.
4. D. Antoine and A. Morel, *A multiple scattering algorithm for atmospheric correction of remotely sensed ocean colour (meris instrument): Principle and implementation for atmospheres carrying various aerosols including absorbing ones*, International Journal of Remote Sensing **20** (1999), no. 9, 1875-1916.
5. S. Richard, V. Jérôme and R. Didier, *Meris level 2 products over land: Validation and potential improvements*, International Geoscience and Remote Sensing Symposium (IGARSS) **3** (2003), 1594-1596.
6. P. J. Curran and C. M. Steele, *Terrestrial meris*, International Geoscience and Remote Sensing Symposium (IGARSS) **6** (2001), 2651-2653.
7. C. Schmechtig, V. Carrère, P. Dubuisson, J. C. Roger and R. Santer, *Sensitivity analysis for the aerosol retrieval over land for meris*, International Journal of Remote Sensing **24** (2003), no. 14, 2921-2944.
8. D. Ramon, R. Santer and J. Vidot, *Meris level 2 products over land: Present status and potential improvements*, Proceedings of SPIE - The International Society for Optical Engineering **4891** (2002), 217-226.
9. G. Levrini and G. Brooker, *Enviview: A gateway to access the envisat data products*, Earth Observation Quarterly (2001), no. 68, 8-11.
10. S. Badessi, H. L. Moeller, P. Viau, D. Castrovillari and B. Collini-Nocker, *The envisat data dissemination system*, European Space Agency Bulletin (2002), no. 109, 12-19.
11. P. Goryl and J. P. Huot, *Overview of the envisat meris and aatsr data quality, calibration and validation program*, International Geoscience and Remote Sensing Symposium (IGARSS) **3** (2003), 1588-1590.
12. G. B. Courrèges-Lacoste, J. G. Schaarsberg, R. Sprik and S. Delwart, *Modeling of spectralon diffusers for radiometric calibration in remote sensing*, Optical Engineering **42** (2003), no. 12, 3600-3607.
13. S. Delwart and L. Bourg, *Meris 1st year: Early calibration results*, International Geoscience and Remote Sensing Symposium (IGARSS) **3** (2003), 1591-1593.
14. M. Kneubuehler, M. E. Schaepman, D. Schlöpfer and K. J. Thome, *Meris / envisat vicarious calibration over land*, Proceedings of SPIE - The International Society for Optical Engineering, 2004, pp. 614-623.
15. J. Nieke, M. Hori, T. Aoki, T. Tanikawa, H. Motoyoshi and Y. Nakajima, *Cross-calibration of satellite sensors over snow fields*, Proceedings of SPIE - The International Society for Optical Engineering, 2003, pp. 406-414.
16. Y. M. Govaerts and M. Clerici, *Evaluation of radiative transfer simulations over bright desert calibration sites*, IEEE Transactions on Geoscience and Remote Sensing **42** (2004), no. 1, 176-187.
17. W. A. Abdou, C. J. Bruegge, M. C. Helmlinger, J. E. Conel, S. H. Pilorz, W. Ledeboer, B. J. Gaitley and K. J. Thome, *Vicarious calibration experiment in support of the multi-angle imaging spectroradiometer*, IEEE Transactions on Geoscience and Remote Sensing **40** (2002), no. 7, 1500-1511.
18. P. M. Teillet, D. N. H. Horler and N. T. O'Neill, *Calibration, validation, and quality assurance in remote sensing: A new paradigm*, Canadian Journal of Remote Sensing **23** (1997), no. 4, 401-414.
19. P. M. Teillet, G. Fedosejevs, R. P. Gauthier, N. T. O'Neill, K. J. Thome, S. F. Biggar, H. Ripley and A. Meygret, *A generalized approach to the vicarious calibration of multiple earth observation sensors using hyperspectral data*, Remote Sensing of Environment **77** (2001), no. 3, 304-327.
20. A. Berk, L. S. Bernstein, G. P. Anderson, P. K. Acharya, D. C. Robertson, J. H. Chetwynd and S. M. Adler-Golden, *Modtran cloud and multiple scattering upgrades with application to aviris*, Remote Sensing of Environment **65** (1998), no. 3, 367-375.
21. F. X. Kneisys, L. W. Abreu, G. P. Anderson, J. H. Chetwynd, E. P. Shettle, A. Berk, L. S.

- Bernstein, D. C. Robertson, P. K. Acharya, L. S. Rothman, S. J.E.A., W. O. Gallery and S. A. Clough, "The modtran 2/3 and lowtran 7 model," Ontar Corporation, North Andover, MA, 1995.
22. G. Hazeu, "The dutch land use database lgn," <http://www.alterra.wur.nl/UK/cgi/LGN/>, 2004.
  23. Y. H. Hu, H. B. Lee and F. L. Scarpace, *Optimal linear spectral unmixing*, Ieee Transactions on Geoscience and Remote Sensing **37** (1999), no. 1, 639-644.
  24. A. A. Nielsen, *Spectral mixture analysis: Linear and semi-parametric full and iterated partial unmixing in multi- and hyperspectral image data*, International Journal of Computer Vision **42** (2001), no. 1-2, 17-37.
  25. J. C. Harsanyi and C. I. Chang, *Hyperspectral image classification and dimensionality reduction - an orthogonal subspace projection approach*, Ieee Transactions on Geoscience and Remote Sensing **32** (1994), no. 4, 779-785.